A compact interferometer insensitive to scanning speed variations

Qinghua Yang (杨庆华)[1*], Baochang Zhao (赵葆常)[2], and Xiaodong Zeng (曾晓东)[1]

[1]*School of Technical Physics, Xidian University, Xi'an 710071, China*

[2]*Xi'an Institute of Optics and Precision Mechanics, Chinese Academy of Sciences, Xi'an 710119, China*

[*]*Corresponding author: yangqh666@163.com*

Received June 18, 2012; accepted August 7, 2012; posted online January 21, 2013

A compact moving optical-wedge interferometer (CMOWI) is presented. This device consists of a moving optical wedge (MOW), a fixed optical wedge (FOW), a fixed compensating plate, and a beam-splitting cube. The optical path difference (OPD) is calculated and analyzed. The factor between the OPD and the displacement of the MOW is less than 1 if the refractive index and wedge angle of the MOW and FOW are chosen properly. Therefore, the CMOWI is insensitive to scanning speed variations compared with the traditional Michelson interferometer. The CMOWI is compact, small-sized, and suitable for low-resolution Fourier transform spectroscopy.

OCIS codes: 120.3180, 260.3160, 120.6200, 300.6190.

doi: 10.3788/COL201311.021202.

The moving mirror used to vary the optical path difference (OPD) in a two-beam Fourier transform spectrometer is either stepped between sampled positions or driven at a constant speed. Scanning speed variations in the latter method produce errors in the sampled interferogram, i.e., the samples are obtained at unequal increments of the OPD[1]. Small sampling errors occur in practice[1−4]. Mechanical disturbances will also introduce sampling errors even when the speed variation of the moving mirror is negligible[5].

The use of dynamic alignment techniques in the moving mirror is a typical method for reducing the influence of scanning speed variations on sampling errors[6]. The dynamic alignment system continuously measures the absolute velocity of the moving mirror within a very short sampling time during scanning. This system also adjusts the velocity via a particular feedback system. The use of a moving optical wedge is another method for reducing the influence of scanning speed variations on sampling errors[7]. However, the interferometer proposed in Ref. [7] remains complex.

In this letter, we present a compact moving optical-wedge interferometer (CMOWI), which compared with the traditional Michelson interferometer, is insensitive to scanning speed variations. Compared with the interferometer proposed in Ref. [7], the CMOWI is more compact, smaller in size, and easier to assemble and calibrate. The CMOWI also uses a fewer number of optical elements.

Figure 1 shows the optical layout of the CMOWI-1, which is made up of one moving optical wedge (MOW), one fixed optical wedge (FOW), one fixed compensating plate, and one beam-splitting cube formed by two glued identical right-angle prisms. The FOW and the beam-splitting cube are glued together, as well as the compensating plate and the beam-splitting cube. The right-angle surface of the MOW is coated with reflecting films of high reflectivity. The hypotenuse surfaces of the MOW and FOW are parallel. The MOW and the FOW have the same wedge angle α and refractive index n. The compensating plate is a plane-parallel glass plate with the same material as the two optical wedges. The upper surface of the compensating plate is coated with reflecting films of high reflectivity. The MOW moves at a constant speed along its hypotenuse surface, and the OPD is created by the straight reciprocating motion of the MOW.

The beam-splitting cube, the compensating plate, and the FOW can use the same kind of material. In this case, the reflection will not occur on the interface between the beam-splitting cube and the compensating plate (or the FOW). Accordingly, the unexpected interference between the reflective beams of the two surfaces of the beam-splitting cube will be avoided.

The light source transmitted through the collimating lens becomes the parallel beam, which is then divided into two beams at right angles at the semi-reflecting surface of the beam-splitting cube. One beam is reflected at the right-angle surface of the MOW, whereas the other is reflected at the upper surface of the fixed compensating plate. These beams then return to the beam-splitting cube, where they are re-combined to enter the collecting lens. Finally, they are received by the detector to become

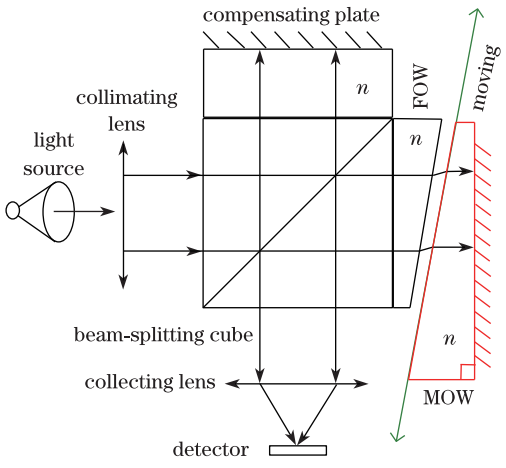

Fig. 1. Optical layout of the CMOWI-1.

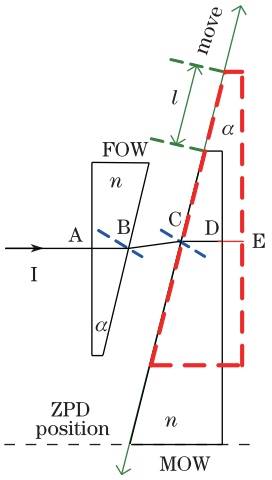

Fig. 2. Ray tracing of the CMOWI-1.

a useful signal.

The OPD (x) as a function of the displacement (l) of the MOW from the zero path difference (ZPD) position is analyzed as follows. Suppose that 1) the MOW is at its ZPD position at time t_1, which is indicated by the black solid line in Fig. 2; 2) the position of the MOW is indicated by the dashed line in Fig. 2 at time $t_1 + t$. The displacement of the MOW from the ZPD position is indicated by l. Figure 2 shows that A is the intersection of ray I and the right-angle surface of the FOW, B is the intersection of ray I and the hypotenuse surface of the FOW, C is the intersection of ray I and the hypotenuse surface of the MOW, D is the intersection of ray I and the right-angle surface of the MOW at time t_1, and E is the intersection of ray I and the right-angle surface of the MOW at time $t_1 + t$.

Figure 2 shows that optical path length (OPL) of ray I from point A to point D (at time t_1, the MOW is at its ZPD position) can be written as

$$\mathrm{OPL}_0 = |\overline{\mathrm{AB}}| \cdot n + |\overline{\mathrm{BC}}| + |\overline{\mathrm{CD}}| \cdot n. \tag{1a}$$

The OPL of ray I from point A to point E (at time $t_1 + t$, the displacement of the MOW from the ZPD position is l) can be written as

$$\mathrm{OPL}_\mathrm{I} = |\overline{\mathrm{AB}}| \cdot n + |\overline{\mathrm{BC}}| + |\overline{\mathrm{CE}}| \cdot n. \tag{1b}$$

Therefore, the OPD x can be written as

$$\begin{aligned} x &= 2 \cdot \mathrm{OPL}_\mathrm{I} - 2 \cdot \mathrm{OPL}_0 = 2 \cdot \left(|\overline{\mathrm{CE}}| - |\overline{\mathrm{CD}}|\right) \cdot n \\ &= 2 \cdot |\overline{\mathrm{DE}}| \cdot n. \end{aligned} \tag{2}$$

Based on the geometrical relationship in Fig. 2, we can get

$$|\overline{\mathrm{DE}}| = l \cdot \sin\alpha. \tag{3}$$

Substituting Eq. (3) into Eq. (2), we can obtain

$$x = 2nl \sin\alpha. \tag{4}$$

Equation (4) can also be written as

$$x = F \cdot l, \tag{5}$$

where the factor F between OPD x and MOW displacement l can be written as

$$F = 2n \sin\alpha. \tag{6}$$

Figures 3(a) and (b) show the graph of factor F that is relative to refractive index n and wedge angle α, which indicates that the factor F increases with the increased n, α, or both. We can obtain $F < 1$ if the values of n and α are chosen properly.

The factor F' between the OPD and the displacement of the moving mirror in a traditional Michelson interferometer is equal to 2, i.e., $F' = 2$. Therefore, the CMOWI is insensitive to scanning speed variations compared with the traditional Michelson interferometer if the wedge angle α and refractive index n of the MOW and FOW are selected properly.

The MOW can also move at a constant speed along its right-angle surface to create OPD. Figure 4 shows the optical layout of the CMOWI-2. The compensating plate and the beam-splitting cube are glued together, as well as the FOW and the beam-splitting cube.

The OPD of the CMOWI-2 is analyzed as follows. Figure 5 shows points A, B, C, and D, which are respectively defined in Fig. 2. The intersection of ray I and the hypotenuse surface of the MOW at time $t_1 + t$ is denoted by G; H is the intersection of ray I and the right-angle surface of the MOW at time $t_1 + t$; θ is the angle of refraction of ray I on the hypotenuse surface of the FOW.

Figure 5 indicates that the OPL from point B to point D (at time t_1, the MOW is at its ZPD position) can be

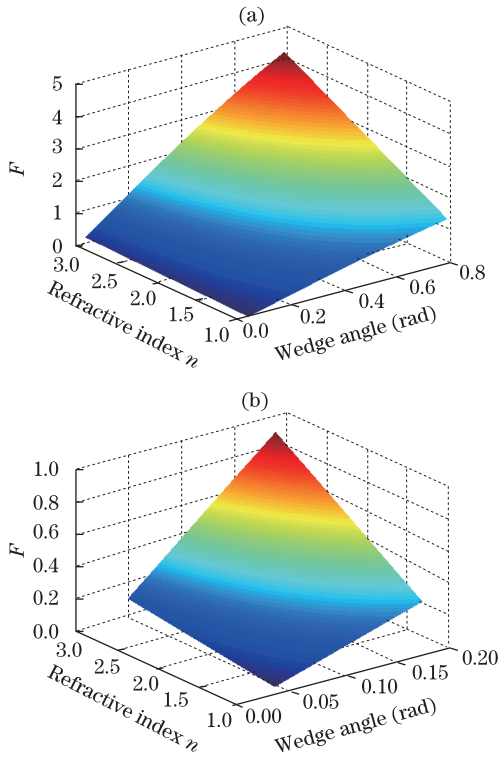

Fig. 3. Graph of factor F relative to refractive index n and wedge angle α. (a) $\alpha \in [\pi/90, \pi/4]$ and (b) $\alpha \in [\pi/90, \pi/18]$.

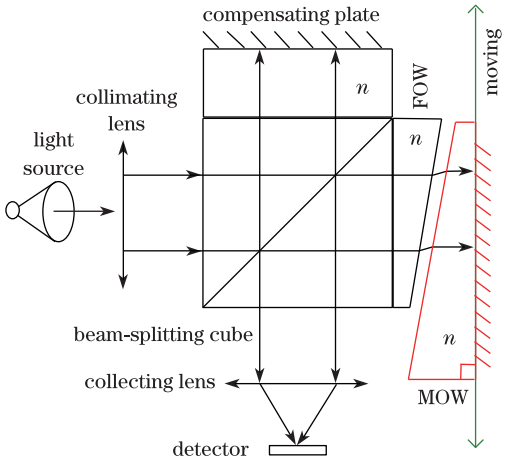

Fig. 4. Optical layout of the CMOWI-2.

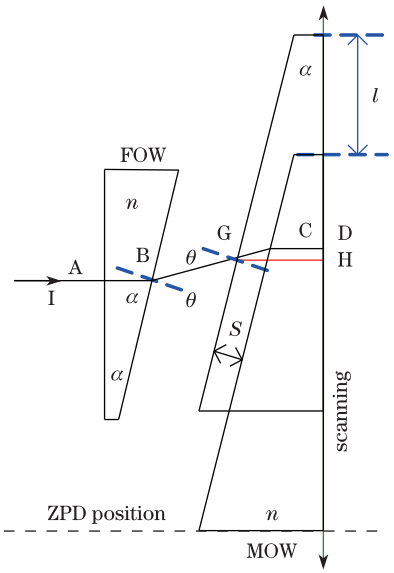

Fig. 5. Ray tracing of the CMOWI-2.

written as

$$\mathrm{OPL}'_0 = \left|\overline{\mathrm{BC}}\right| + \left|\overline{\mathrm{CD}}\right| \cdot n = \left|\overline{\mathrm{BG}}\right| + \left|\overline{\mathrm{GC}}\right| + \left|\overline{\mathrm{CD}}\right| \cdot n. \tag{7a}$$

The OPL from point B to point H (at time $t_1 + t$, the displacement of the MOW from the ZPD position is l) can be written as

$$\mathrm{OPL}' = \left|\overline{\mathrm{BG}}\right| + \left|\overline{\mathrm{GH}}\right| \cdot n. \tag{7b}$$

Therefore, the OPD can be written as

$$\begin{aligned} x &= 2 \cdot \mathrm{OPL}' - 2 \cdot \mathrm{OPL}'_0 \\ &= 2n\left(\left|\overline{\mathrm{GH}}\right| - \left|\overline{\mathrm{CD}}\right|\right) - 2\left|\overline{\mathrm{GC}}\right|. \end{aligned} \tag{8}$$

Based on the law of refraction and geometrical relationship in Fig. 5, we have

$$n \sin\alpha = \sin\theta, \tag{9a}$$

$$s = l \sin\alpha, \tag{9b}$$

$$\left|\overline{\mathrm{GC}}\right| = \frac{s}{\cos\theta} = \frac{l\sin\alpha}{\cos\theta}, \tag{9c}$$

$$\left|\overline{\mathrm{GH}}\right| - \left|\overline{\mathrm{CD}}\right| = \left|\overline{\mathrm{GC}}\right| \cos(\theta - \alpha). \tag{9d}$$

Substituting Eqs. (9a)–(9d) into Eq. (8), we can obtain

$$\begin{aligned} x &= 2n\left|\overline{\mathrm{GC}}\right| \cos(\theta - \alpha) - 2\left|\overline{\mathrm{GC}}\right| \\ &= 2n\frac{l\sin\alpha}{\cos\theta}(\cos\theta\cos\alpha + \sin\theta\sin\alpha) - 2\frac{l\sin\alpha}{\cos\theta} \\ &= \left(n\sin 2\alpha + \frac{2n^2\sin^3\alpha - 2\sin\alpha}{\sqrt{1 - n^2\sin^2\alpha}}\right) \cdot l \quad . \end{aligned} \tag{10}$$

Equation (10) can be rewritten as

$$x = K \cdot l, \tag{11}$$

where the factor K between OPD x and MOW displacement l can be written as

$$K = n\sin 2\alpha + \frac{2n^2\sin^3\alpha - 2\sin\alpha}{\sqrt{1 - n^2\sin^2\alpha}}. \tag{12}$$

Figure 6 shows the graph of factor K relative to refractive index n and wedge angle α. Factor K increases with the increased n, α, or both.

The misalignment of the MOW generates a small OPD error. Figure 7 shows the equivalent sketch map of the light path when the MOW is tilted. Figure 7 defines points A, B, C, and D. Figure 2 indicates that points E, F, M, and N are the intersections of the deflected ray and the MOW and the FOW and the beam-splitting cube, respectively. L is the length of light path from the bottom of beam-splitting cube to the detector; $2a$ is the side length of the beam-splitting cube; d is the distance between the two right-angle surfaces of the FOW and MOW; s_0 is the distance between the two hypotenuse surfaces of the FOW and MOW; θ' is the angle of refraction of the deflected ray on the hypotenuse surface of the MOW; δ is the angle of refraction of the deflected ray on the right-angle surface of beam-splitting cube; φ is the tilt angle of the MOW.

Based on the geometrical relationship in Fig. 7, we have

$$\left|\overline{\mathrm{BC}}\right| = \frac{s_0}{\cos\theta}, \tag{13a}$$

$$\left|\overline{\mathrm{EF}}\right| = \frac{s_0}{\cos\theta'}, \tag{13b}$$

$$\left|\overline{\mathrm{AB}}\right| + \left|\overline{\mathrm{CD}}\right| = d - \left|\overline{\mathrm{BC}}\right| \cos(\theta - \alpha). \tag{13c}$$

The OPD error resulting from the misalignment of the MOW can be written as

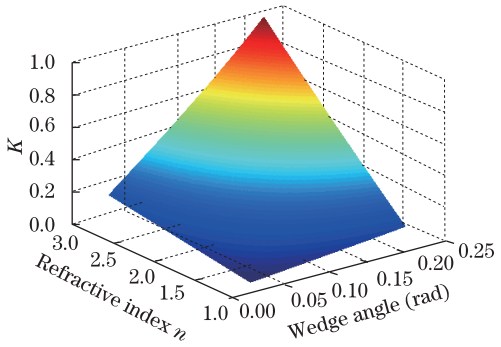

Fig. 6. Graph of factor K relative to refractive index n and wedge angle α.

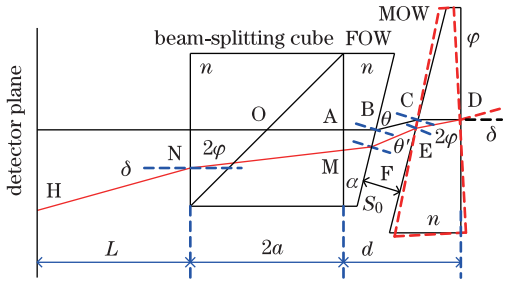

Fig. 7. Equivalent sketch map of the light path with tilted MOW.

$$\begin{aligned}\Delta x &= n\cdot\left[\left(\left|\overline{\mathrm{DE}}\right|+\left|\overline{\mathrm{FM}}\right|\right)-\left(\left|\overline{\mathrm{AB}}\right|+\left|\overline{\mathrm{CD}}\right|\right)\right]\\&\quad+\left[\left|\overline{\mathrm{EF}}\right|-\left|\overline{\mathrm{BC}}\right|\right]\ +n\cdot\left[\left|\overline{\mathrm{MN}}\right|-2\mathrm{a}\right]+\left[\left|\overline{\mathrm{NH}}\right|-L\right]\\&\approx n\cdot\left[\frac{\left|\overline{\mathrm{AB}}\right|+\left|\overline{\mathrm{CD}}\right|}{\cos(2\varphi)}-\left(\left|\overline{\mathrm{AB}}\right|+\left|\overline{\mathrm{CD}}\right|\right)\right]\\&\quad+\left[\left|\overline{\mathrm{EF}}\right|-\left|\overline{\mathrm{BC}}\right|\right]\ +n\cdot\left[\left|\overline{\mathrm{MN}}\right|-2\mathrm{a}\right]+\left[\left|\overline{\mathrm{NH}}\right|-L\right]\\&=n\cdot\left[d-s_0\left(\cos\alpha+\frac{\sin\theta\sin\alpha}{\cos\theta}\right)\right]\cdot\left[\frac{1}{\cos(2\varphi)}-1\right]\\&\quad+\left[\frac{s_0}{\cos\theta'}-\frac{s_0}{\cos\theta}\right]+n\cdot\left[\frac{2\mathrm{a}}{\cos(2\varphi)}-2\mathrm{a}\right]+\left[\frac{L}{\cos\delta}-L\right].\end{aligned}\tag{14}$$

Based on the law of refraction, we have

$$n\sin\alpha=\sin\theta,\tag{15a}$$
$$n\sin(\alpha+2\varphi)=\sin\theta',\tag{15b}$$
$$n\sin(2\varphi)=\sin\delta.\tag{15c}$$

Therefore, the small OPD error resulting from the misalignment of the MOW can be expressed as

$$\begin{aligned}\Delta x\approx n\cdot&\left[2\mathrm{a}+d-s_0\left(\cos\alpha+\frac{n\sin^2\alpha}{\sqrt{1-n^2\sin^2\alpha}}\right)\right]\\&\cdot\left[\frac{1}{\cos(2\varphi)}-1\right]+s_0\left[\frac{1}{\sqrt{1-n^2\sin^2(\alpha+2\varphi)}}-\frac{1}{\sqrt{1-n^2\sin^2\alpha}}\right]\\&+L\cdot\left[\frac{1}{\sqrt{1-n^2\sin^2(2\varphi)}}-1\right].\end{aligned}\tag{16}$$

Suppose that 1) b_1 is the side length of right-angle side of the FOW; 2) a_1 and $a_1+b_1\tan\alpha$ are the side lengths of the two bases of the FOW, respectively; 3) b_2 ($b_2>b_1$) is the side length of right-angle side of the MOW; and 4) a_2 and $a_2+b_2\tan\alpha$ are the side lengths of the two bases of the MOW, respectively.

The effective maximum displacement of the MOW of the CMOWI-1 is

$$\begin{aligned}l_{e\max}&=\frac{(a_1+a_2+b_2\tan\alpha)-(a_1+b_1\tan\alpha+a_2)}{\sin\alpha}\\&=\frac{b_2-b_1}{\cos\alpha}.\end{aligned}\tag{17}$$

Thus, the effective OPD range of the CMOWI-1 can be written as

$$x_{e\max}=2n\sin\alpha\cdot l_{e\max}=2n(b_2-b_1)\tan\alpha.\tag{18}$$

The effective maximum displacement of the MOW of the CMOWI-2 is

$$l_{e\max}=b_2-b_1.\tag{19}$$

Thus, the effective OPD range of the CMOWI-2 can be written as

$$\begin{aligned}x_{e\max}&=\left(n\sin 2\alpha+\frac{2n^2\sin^3\alpha-2\sin\alpha}{\sqrt{1-n^2\sin^2\alpha}}\right)\cdot l_{e\max}\\&=\left(n\sin 2\alpha+\frac{2n^2\sin^3\alpha-2\sin\alpha}{\sqrt{1-n^2\sin^2\alpha}}\right)\cdot(b_2-b_1).\end{aligned}\tag{20}$$

In conclusion, the CMOWI is expounded, and its properties are analyzed. The factor F between the OPD and the displacement of the MOW increases with the increasing of either the wedge angle α, or the refractive index n, or both. $F<1$ can be obtained if the values of n and α are chosen properly. The OPD can be lesser than the displacement of the MOW if the values of n and α are chosen properly. Therefore, the CMOWI is insensitive to scanning speed variations compared with the traditional Michelson interferometer if the refractive index n and wedge angle α of the two optical wedges are selected properly. The CMOWI is compact, small-sized, and suitable for low resolution Fourier transform spectroscopy.

References

1. A. S. Zachor, Appl. Opt. **16,** 1412 (1977).
2. A. S. Zachor and S. M. Aaronson, Appl. Opt. **18,** 68 (1979).
3. D. L. Cohen, Appl. Opt. **38,** 139 (1999).
4. L. Palchetti and D. Lastrucci, Appl. Opt. **40,** 3235 (2001).
5. B. Saggin, L. Comolli, and V. Formisano, Appl. Opt. **46,** 5248 (2007).
6. T. Yoshimura, Y. Syoji, and N. Wakabayashi, J. Phys. E **10,** 829 (1977).
7. Q. Yang, R. Zhou, and B. Zhao, Appl. Opt. **47,** 2186 (2008).